Applied Surface Science 614 (2023) 156229

Contents lists available at ScienceDirect

Applied Surface Science

journal homepage: www.elsevier.com/locate/apsusc

Full Length Article

In-situ surface defects passivation with small carbon chain molecules for highly efficient, air-processed inorganic $CsPbI_2Br$ perovskite photovoltaics

Jitendra Bahadur [a,1], Jun Ryu [b,1], Dong-Gun Lee [b], Jongin Hong [b,c], Shuzi Hayase [d], Jung Sang Cho [e,*], Sang Mun Jeong [f,*], Dong-Won Kang [a,b,*]

[a] Department of Energy Systems Engineering, Chung-Ang University, Seoul 06974, Republic of Korea
[b] Department of Smart City, Chung-Ang University, Seoul 06974, Republic of Korea
[c] Department of Chemistry, Chung-Ang University, Seoul 06974, Republic of Korea
[d] Info-Powered Energy System Research Center, The University of Electro-Communications, 1-5-1 Chofugaoka, Chofu, Tokyo 182-8585, Japan
[e] Department of Engineering Chemistry, Chungbuk National University, 1 Chungdae-Ro, Seowon-Gu, Cheongju-si, Chungbuk 361-763, Republic of Korea
[f] Department of Chemical Engineering, Chungbuk National University, Cheongju 28644, Republic of Korea

ARTICLE INFO

Keywords:
Additive engineering
Crystal growth
Surface defects
Inorganic
Perovskite solar cell

ABSTRACT

All-inorganic $CsPbI_2Br$ perovskites have gained enormous interests owing to suitable band gap and thermal stability. However, the $CsPbI_2Br$ suffers from unsatisfactory crystal growth and poor surfaces processed under ambient conditions. Herein, we introduced small carbon chain molecules as liquid additives including diiodomethane (DIM), dibromoethane (DBM), and dichloromethane (DCM) into the precursor. The halide ions as associated with these additives played vital roles to passivate the surface defects. Interestingly, DIM additive offers multiple benefits: (i) passivate uncoordinated Pb^{2+} dangling bonds (ii) match band energy alignment, (iii) assist to preferential oriented crystal growth (iv) suppress halide ion vacancies and (v) improve surface morphology. As a result, 100 μl DIM-assisted perovskite solar cell (PSC) exhibited the highest power conversion efficiency (PCE) of 16.42 % which is higher than that of control (13.95 %). Notably, with additive engineering approach our champion PCE (16.42 %) is the highest to date under processing at ambient conditions. On the contrary to poor stability of control PSC (PCE drop of ~ 50 %), the DIM assisted PSC retained ~ 80 % of original PCE after aging for 600 hrs. Thus, our photovoltaic results demonstrated that the additive method could open an effective route for development of efficient and stable PSCs under ambient conditions.

1. Introduction

Organic-inorganic hybrid perovskites have gained extensive attention due to their excellent optoelectronic properties including higher optical absorption, high carrier mobility, tunable optical band gap, long charge carrier diffusion length. [1–3] Also, their low cost and solution processability make them the most promising photovoltaic material for next generation solar cell. The power conversion efficiency (PCE) of perovskite solar cells (PSCs) is rapidly increased from 3.8 % [4] to a certified value of 25.7 %, [5] approaching PCE value of single crystalline silicon based solar cell. [6] However, major issues associated with organic cations (methylammonium ion (MA^+) or formamidinium ion (FA^+)) are volatile and thermally unstable nature, leading to poor structural stability. [2] Thus, it is necessary to resolve these issues by replacing the organic cations with inorganic cations in perovskite structure. In this regard, all inorganic perovskite $CsPbX_3$ (X = Cl, I, and Br or mixed halides) structures have been developed, [7,8] in which organic cation is replaced with inorganic cation cesium (Cs) and having unique optoelectronic properties as almost comparable to organic–inorganic hybrid perovskites with excellent thermal and photostability. [9] The inorganic cation Cs^+ ion not only forms stable phase of $CsPbX_3$ (greater than 300℃), but also provides an adjustable optical band edge from 1.73 eV to 2.30 eV, which is suitable for use as a top cell in fabrication of tandem solar cell. [10,11] Recently, all inorganic $CsPbI_3$ based PSC achieved a PCE of 20.7 %. [12] However, $CsPbI_3$ suffers from phase transformation as photoactive cubic perovskite structure (black α-phase) easily degrades into photo inactive orthorhombic non-perovskite (δ-phase) structure at room temperature or under ambient

* Corresponding authors at: Department of Energy Systems Engineering, Chung-Ang University, Seoul 06974, Republic of Korea (D.-W. Kang).
E-mail addresses: jscho@cbnu.ac.kr (J. Sang Cho), smjeong@chungbuk.ac.kr (S. Mun Jeong), kangdwn@cau.ac.kr (D.-W. Kang).
[1] J. Bahadur and J. Ryu contributed equally.

https://doi.org/10.1016/j.apsusc.2022.156229
Received 2 October 2022; Received in revised form 9 December 2022; Accepted 22 December 2022
Available online 26 December 2022

conditions. [13] On the other hand, inorganic perovskites, $CsPbBr_3$ and $CsPbCl_3$, exhibit better phase stability under ambient conditions, [3,10] however, their larger optical band edges limit the light harvesting properties.

$CsPbI_2Br$ has been considered as a promising light absorbing material to develop efficient PSCs owing to its an optimal bandgap (~1.92 eV), higher tolerance factor and favorable intrinsic phase stability. [8,10,14,15] Unfortunately, $CsPbI_2Br$ film still suffers from poor crystallization and unwanted phase transition under higher humid conditions, [7] which are big challenges for development of efficient $CsPbI_2Br$ PSCs. One-step solution approach is widely adopted for fabrication of $CsPbI_2Br$ based PSCs, [16,17] however in this method, owing to unsatisfactory crystallization and heterogeneous growth, poor quality perovskite film is formed with random orientation of grains, irregular grains size, pin holes, voids, and rough surface [7,18] that act as defects, resulting reduced the device performance. Therefore, it is essential to prepare high crystalline $CsPbI_2Br$ film with desirable surface topography for efficient device fabrication. The various strategies including interfacial engineering, [19–22] doping including cation and metal, [23–27] gradient thermal annealing, [7,28] additive engineering, [9,29,30] precursor solvent and antisolvent engineering [1,31–33] have been introduced to regulate the crystal growth, improve the crystallinity, and surface morphology of $CsPbI_2Br$ film. Among these, additive engineering is a most effective approach to tune the microstructure and morphology of $CsPbI_2Br$ film, because inorganic perovskite easily interacts with other functional groups (covalent and ionic), owing to its ionic-covalent feature. Moreover, additives are not only to modulate the crystallization kinetics by accelerating the nucleation and retarding the crystallization process, but also to play a crucial role to passivate the defects through coordinating the dangling bonds. [30] For instance, Fu et al. has used 2-hydroxyethyl methacrylate (HEMA) as an additive for fabrication of high crystalline $CsPbI_2Br$ film and achieved device PCE of 16.13 %. [9] Yu and his co-workers employed thioacetamide with S donor (TAA) and acetamide with O donor (AA) to manipulate the crystallization process of $CsPbI_2Br$ film and found device PCE of 15.87 % and 15.02 %, respectively. [34] Li et al. has developed an efficient $CsPbI_2Br$ based PSC with PCE of 15.59 % by introducing guanidinobenzoic-acid hydrochloride (GBACl) into perovskite precursor solution. [35] Additionally, Cai et al. has prepared $CsPbI_2Br$ PSC by directly adding polyethyleneimine (PEI) into perovskite precursor solution and exhibited the device PCE of 15.48 %. [36] Consequently, from above literatures, it has been revealed that additive engineering plays an indispensable role to tailor crystallization process for formation of high-quality $CsPbI_2Br$ perovskite film. Furthermore, it should be noted that most of the reported research works with high PCE have been developed in N_2 filled glovebox. However, from mass production aspect, it is essential to develop inorganic $CsPbI_2Br$ PSCs with an efficient photovoltaic performance under ambient conditions. As we have opted dual structure (SnO_2/ZnO) for electron extraction and transportation phenomena in the present work. The conduction band minimum (CBM) position of ZnO (- 4.21 eV) [37] facilitates a well-matched band energy alignment with $CsPbI_2Br$ perovskite to extract the photogenerated electrons. Moreover, the insertion of ZnO layer between SnO_2 and perovskite enables desirable cascade energy band between dual structure (SnO_2/ZnO) electron transport layer (ETL) and perovskite layer, which is more beneficial to extract and transport the photogenerated electrons from perovskite film to indium doped tin oxide (ITO) electrode. [37,38] Thus, dual structure of charge transport layer is an essential approach to reduce the energy loss within the perovskite solar cells.

In the present work, firstly we have introduced diiodomethane (DIM), dibromoethane (DBM), and dichloromethane (DCM) as liquid additives into all-inorganic $CsPbI_2Br$ to fabricate highly crystalline, compact, and uniform $CsPbI_2Br$ perovskite film under air atmospheric conditions. The small carbon chain molecules (DIM, DBM and DCM) would not only tune the optoelectronic properties of $CsPbI_2Br$ film by variation of mixed halide composition, but also diminish the defects through filling the halide ion vacancies and suppress the uncoordinated Pb^{2+} surface traps. It was found that $CsPbI_2Br$ perovskite film quality enhanced with addition of DIM and DCM. However, in case of DBM, the film properties were deteriorated due to formation of additional perovskite phase. The device PCE of 13.95 %, 16.42 %, 12.51 % and 14.45 % were obtained corresponding to control, DIM, DBM and DCM additives-based PSCs. Comparatively, DIM assisted PSC exhibited impressive device performance due to formation of high crystalline, uniform and pinhole free $CsPbI_2Br$ perovskite film. The addition of DIM plays an effective role to enhance highly oriented grain growth and modulate band alignment energy level of $CsPbI_2Br$ perovskite film that improving the device performance. Thus, our work suggests a practical guideline how to produce efficient inorganic $CsPbI_2Br$ PSCs under ambient conditions.

2. Results and discussion

The high crystalline $CsPbI_2Br$ perovskite film with uniform and compact morphology exhibits an efficient photovoltaic performance. Therefore, it is necessary to develop high quality $CsPbI_2Br$ film for efficient fabrication of PSCs. This study focuses on additive engineering in which small carbon chain molecules including DIM, DBM and DCM were used as an additive to modulate the $CsPbI_2Br$ perovskite film properties. Chueh et.al suggested that longer alky chain affects the solute–solvent interaction, resulted in degradation of the device performance. [39] Thus, we have chosen DIM, DBM and DCM molecules owing to presence of small carbon chain (CH_2–). Interestingly, it was found that DIM plays an effective role to improve the film quality that leading to higher performance. The interaction of DIM with inorganic perovskite can be explained using hard and soft acids and bases (HSAB) theory, [40,41] which is well known to illustrate the inorganic and organic chemical reactions. It describes negative ions as alkalis and positive ions as acids and determines absolute chemical hardness using the following equation: [40]

$$\eta = (I_e - A)/2 \quad (1)$$

where, η is absolute chemical hardness, I_e is ionization energy and A is electron affinity. The alkalis and acids can form bonds with equivalent hardness. With HSAB hypothesis, Pb can be considered as acids and I as alkalis, and their η values are 3.53 eV and 3.69 eV, respectively. [40] According to their chemical hardness values, they are likely to respond with one another. Thus, iodide associated with DIM regarded as a ligand and interacts as soft lewis base with Pb^{2+}, soft lewis acid.

Consistent with above hypothesis, iodide ions of DIM additive would passivate the uncoordinated Pb^{2+} ions during perovskite crystal growth and regulate the crystallization kinetics process. Therefore, we can propose that DIM passivates defects like uncoordinated Pb^{2+} ions and suppress the halide ion vacancies in the inorganic perovskite film.

In addition to this, DIM, DBM and DCM consist of C-X (X = I, Br, and Cl) bonds that might be cleaved during thermal annealing and participate in perovskite crystal formation by releasing extra free halide ions as shown in Fig. 1 (a). As $CsPbI_2Br$ perovskites already consist of I^- and Br^- halide ions, to confirm the presence of extra halide ions in the prepared perovskite film, we conducted the X-ray photoelectron spectroscopy (XPS) analysis for the control perovskite and films with DCM additive that contains the different halide ions (Cl^-). The obtained high-resolution patterns corresponding to Cs, Pb, I, Br and Cl core levels are depicted in Fig. S1 (a-e), respectively. A negligible shift has been found in the peak position of Cs, Pb, I, and Br core levels with DCM additive, which suggested that Cl^- ions are not entering into crystal lattice. Notably, Cl 2p peak is found in the DCM additive-based perovskite film as compared to control film as shown in Fig. S1 (e), indicating the existence of Cl^- ions at the surface of DCM assisted perovskite films. Liu and his co-workers have revealed that Cl^- ions do not incorporate into $CsPbI_2Br$ crystal lattice. [42] They confirmed that Cl^- ions present on the surface of perovskite film. Moreover, it has been demonstrated that Cl^- ions located

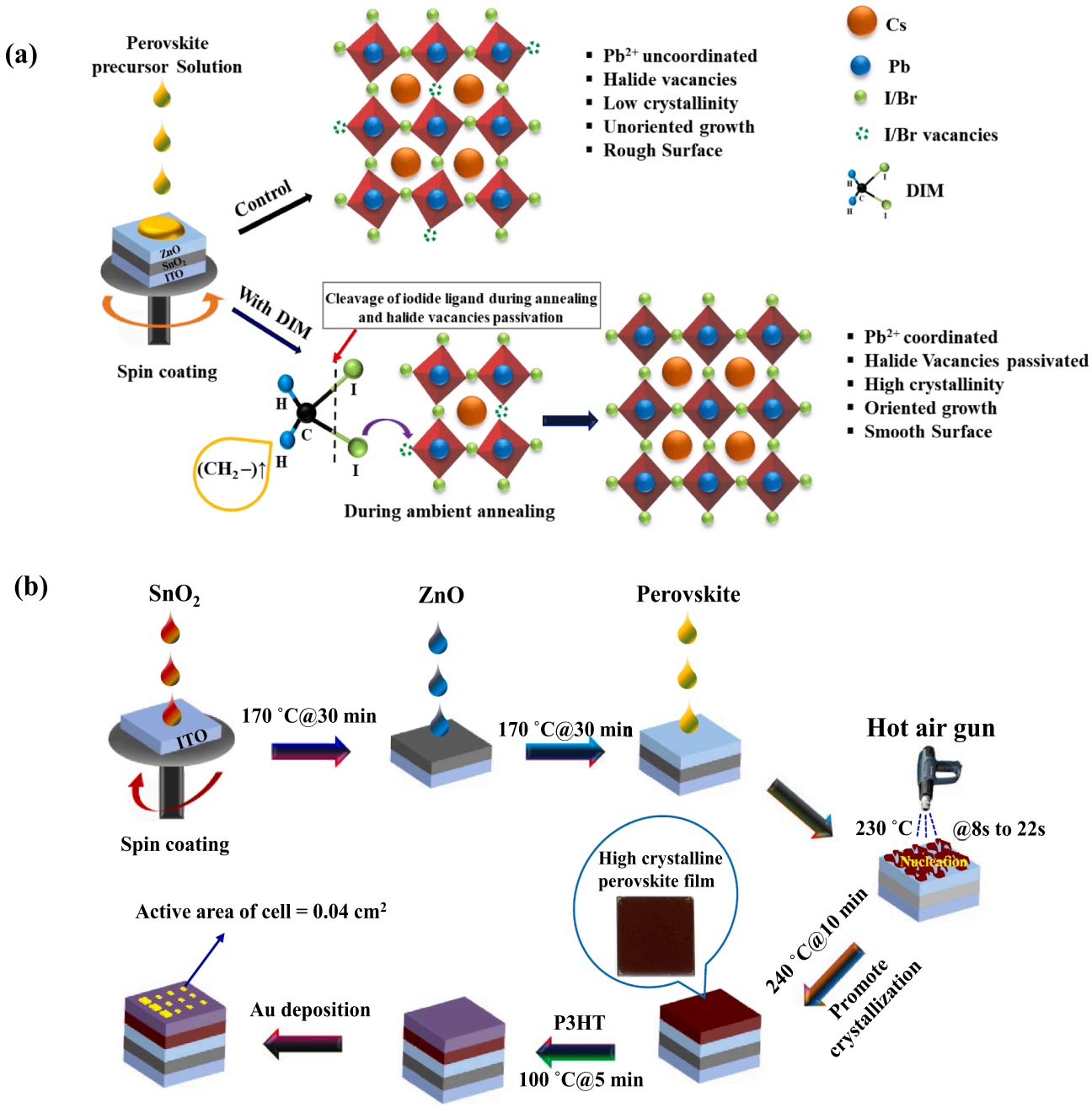

Fig. 1. Schematic representation for **(a)** Role of DIM additive to suppress the halide vacancies within the perovskite film and **(b)** Fabrication of inorganic $CsPbI_2Br$ perovskite solar cell in atmospheric air.

in the grain boundaries of perovskite film. [43,44] Therefore, it has been clearly revealed that Cl^- ions present on the surface of DCM assisted perovskite film, which was annealed at 240 °C for 10 min under ambient atmosphere. It is worth to note that DCM has low boiling point (40 °C) and Cl^- ions are still present on the surface of resulting perovskite film. That means DIM (boiling point of 181 °C) and DBM (boiling point of 96.95 °C) additives would also supply the extra free halide ions in the perovskite formation. Therefore, we can suggest that C-X bond of DIM, DBM and DCM would be dissociated, and extra free halide ions play a key role to modulate the perovskite crystal growth process. Moreover, as perovskite films are annealed at 240 °C for 10 min under ambient environment, so it can be predicted that residual of part (CH_2–) of these additives might be evaporated. Furthermore, the C-X bond strength is different owing to dissimilar electronegativity of each halogen atom (X = I^-, Br^- or Cl^-). It has been demonstrated that C-X bond strength decreases in order of C-Cl (78 kcal mol^{-1}) > C-Br (68 kcal mol^{-1}) > C-I (51 kcal mol^{-1}), and C-X bond can be dissociated by thermal energy. For instance, Chueh et.al clearly suggested that C-X (X = I-, Br- or Cl-) bond is cleaved during thermal annealing process and released free halide ions participate in perovskite crystal formation. [39] In addition, Gao et al. have also been suggested that organic halide salts (phenylethylammonium iodide (PEAI, melting point = 283 °C) and phenylethylammonium bromide (PEABr, melting point = 270 °C) filled the halide ion vacancies by providing extra halide anions at high temperature annealing (300 °C). [45].

The digital photograph of prepared perovskite solutions with each concentration of DIM, DBM and DCM and corresponding quality of fabricated perovskite films are shown in Fig. S2 (a), Fig. S2 (b), and Fig. S2(c), respectively. It is noted that the color of perovskite precursor solution was changed from light yellow to dark yellow clear transparent

solution with increasing concentration of DIM (25 µl, 50 µl, 100 µl, and 150 µl) as depicted in Fig. S2(a), which revealed that DIM interacted with control $CsPbI_2Br$ precursor solution. In addition, absorbance spectrum was measured corresponding to prepared 25 µl, 50 µl, 100 µl, and 150 µl DIM additive-based precursor solutions to understand the chemical interaction between DIM additive and control $CsPbI_2Br$ precursor solution. As shown in Fig. S3, absorption pattern is shifted with increasing the DIM additive concentration as compared to control, which also confirms that DIM interacted with control $CsPbI_2Br$ precursor solution. In case of DBM (25 µl, 50 µl, and 100 µl), precursor solution is precipitated (Fig. S2(b)). Thus, DBM incorporated $CsPbI_2Br$ perovskite films were fabricated up to 100 µl concentration owing to precipitation of solution. On the other hand, with addition of DCM (25 µl, 50 µl, 100 µl, and 150 µl), color of perovskite precursor solution did not change as shown in Fig. S2(c), because incorporation of Cl^- ions negligibly affects optoelectronic properties. The procedure of PSC fabrication is shown in Fig. 1(b).

The top surface morphology of fabricated $CsPbI_2Br$ film with various additives (DIM, DBM and DCM) was investigated using Field Emission Scanning Electron Microscope (FE-SEM) analysis. The obtained top-view FE-SEM images of control and 100 µl DIM assisted $CsPbI_2Br$ perovskite film are shown in Fig. 2 (a, b). In addition, regarding 25 µl, 50 µl, and 150 µl DIM additives-based $CsPbI_2Br$ perovskite films, FE-SEM images are depicted in Fig. S4. It is clearly observed that the surface morphology of control perovskite film (Fig. 2(a)) is poor with a rough surface. Moreover, control perovskite film exhibited pinholes and large numbers of uneven grains as depicted in cross section FE-SEM image (Fig. 2(c)). The presence of pinholes and grain boundaries is considered as nonradiative recombination centers that affect the device performance. It has been found that with an optimum concentration of DIM additive, pinholes and grain boundaries are significantly suppressed. In detail, with 25 µl and 50 µl DIM concentration, perovskite film quality was improved, while still having rough surface (Fig. S4(a, b)). With increasing DIM concentration to 100 µl, high quality perovskite film is formed with uniform surface (Fig. 2(b)). As further increase DIM concentration (150 µl), morphology of perovskite film is getting degraded (Fig. S4 (c)), which may be owing to higher iodide ions concentration. Thus, with an optimum concentration of DIM (100 µl), $CsPbI_2Br$ perovskite film displays uniform, densely packed, and preferential oriented grain growth perpendicular to substrate as shown in cross section image (Fig. 2(d)) that could be beneficial to obtain efficient device performance. We speculate that DIM additive forms the solid PbX_2-DMSO:DMF-DIM-CsI intermediate phase by partial evaporation of the solvents, which affects the crystal growth dynamics during hot-air treatment. Later the deposited PbX_2-DMSO:DMF-DIM-CsI intermediate phase was annealed at 240 ℃ for 10 min to produce black α-$CsPbI_2Br$ phase. It has been demonstrated that dynamic hot air during spinning process play multiple roles such as assistance to spread the solvent uniformly onto the substrate owing to flow of hot air, and contribution for formation of solid PbX_2-DMSO:DMF-CsI intermediate phase (for $CsPbI_2Br$ film) by partially evaporation of the solvents from precursor solution, which limits nuclei centers and controls the evaporation rate of the solvents. [46] The DIM additive fills the halide vacancies by supplying extra halide anions during perovskite crystal formation. It can be predicted that DIM additive limits nuclei center and modulate the crystallization kinetics, results in improving the film quality. In case of DBM additive, quality of $CsPbI_2Br$ perovskite film is hampered, which may be owing to higher Br concentration. The FE-SEM images for control and DBM with different concentrations (25 µl, 50 µl, and 100 µl) based perovskite films are displayed in Fig. S5. With 25 µl DBM additive, perovskite grains with new phase are observed (Fig. S5 (a)). As an increasing DBM additive (50 µl), an intermediate phase of perovskite was formed (Fig. S5 (b)). Further increase DBM concentration to 100 µl, a very poor-quality perovskite film was obtained with voids and large number of pin holes (Fig. S5(c)). Moreover, at higher concentration of DBM (100 µl), a secondary phase of perovskite with different grains is clearly observed that affects $CsPbI_2Br$ film properties. On the other hand, an optimum concentration of DCM additive improves the film properties. FE-SEM images of $CsPbI_2Br$ perovskite film with different concentration of DCM additive (25 µl, 50 µl, 100 µl and 150 µl) are depicted in Fig. S6. With 25 µl DCM additive, $CsPbI_2Br$ perovskite film morphology is improved (Fig. S6 (a)). As further increasing concentration to 50 µl and 100 µl DCM, perovskite film morphology is slightly roughened as compared to 25 µl DCM additive (Fig. S6(b, c)). While concentration increase to 150 µl DCM, the topography is strongly hampered owing to higher concentration of DCM (Fig. S6(d)). It has been reported that incorporation of Cl^- ions improved the film quality by suppressing the formation of dense nuclei. [47] Thus, an optimum concentration of DCM (25 µl) improved the $CsPbI_2Br$ perovskite film morphology. Comparatively, we can conclude that nuclei to crystal growth mechanism is more favorable with DIM additive that leads to uniform, dense, and pinhole free high quality perovskite film.

To prove the impact of DIM, DBM and DCM additives with various concentrations on crystalline properties of $CsPbI_2Br$ film, X-ray diffraction (XRD) measurement was conducted, and obtained diffraction patterns were displayed in Fig. 2(e), Fig. S7(a) and Fig. S8(a), respectively. The diffraction peaks for control perovskite film at 14.84°, 21.10° and 29.8° can be attributed to (100), (110) and (200) crystal planes, respectively, which confirms the formation of α-$CsPbI_2Br$ phase. [35,48] For DIM assisted perovskite films, it has been found that peak intensity was enhanced as increasing concentration of DIM, suggesting that the crystallinity of α-$CsPbI_2Br$ phase was meliorated. Notably, with 100 µl concentration of DIM, peak intensity corresponding to (200) crystal plane is significantly improved that reveals preferential oriented grain growth. A minor peak shift towards the lower value of 2θ is observed (Fig. 2(f)), which is specifying lattice expansion owing to diffusion of iodide ions from DIM. [49] The d-spacing values (Fig. 2 (g)) corresponding to (200) crystal plane was calculated using Bragg's law ($2d\sin\theta = n\lambda$, where n is diffraction order, d is lattice spacing, θ is scattering angle and λ is incident light wavelength). [50] As a result, increment in d-spacing implies that lattice volume increases by filling the halide vacancies with incorporation of DIM. However, with further increase in the concentration of DIM (150 µl), peak intensity is decreased. Also, the peak position slightly shifted toward higher 2θ value, and reduction in d-spacing as comparison to 100 µl DIM based perovskite film was found, which may be due to excess DIM concentration that deteriorates the crystal properties. For more detailed analysis, full width at half maximum (FWHM), average crystallite size, micro strain and dislocation density were measured using dominant characteristic peak (200). The average crystallite (D) is calculated using Debye-Scherrer equation as following: [51]

$$D = \frac{k\lambda}{\beta cos\theta} \tag{2}$$

where, k is shape factor (~0.9), λ is Cu-K_α wavelength (1.54 Å), β is FWHM (), and θ is scattering angle (). The lower value of FWHM indicates higher crystalline structure. [52] The obtained values of β and D correspond to various concentration of DIM, which are depicted in Fig. 2 (h). It is clearly observed that 100 µl DIM assisted $CsPbI_2Br$ perovskite film exhibited the lowest FWHM and the highest crystallite size, indicating improved crystallinity. In general, micro strain induces in the film owing to presence of various defects including vacancies and interstitial, dislocation, grain boundaries, crystal imperfection and distortion. [53] The micro strain (ε) is obtained using Hall-Williamson equation [51] as mentioned below,

$$\beta cos\theta = \frac{k\lambda}{D} + 4\varepsilon sin\theta \tag{3}$$

$$\varepsilon = \frac{\beta}{4tan\theta} \tag{4}$$

and dislocation density (ρ) is estimated using following equation:

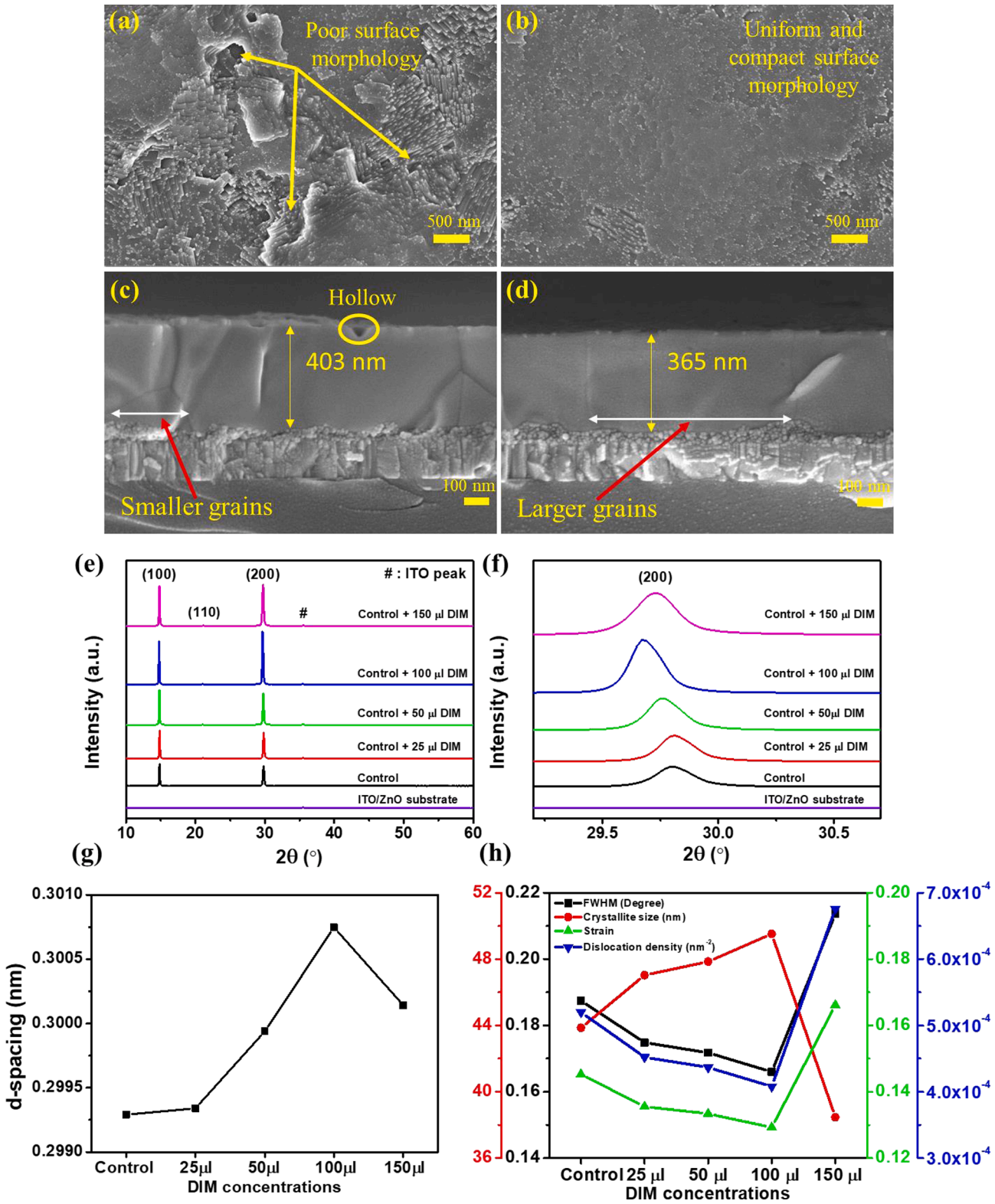

Fig. 2. **(a, b)** Top view FE-SEM images, **(c, d)** Cross section FE-SEM images corresponding to $CsPbI_2Br$ (control) and 100 µl DIM assisted perovskite films deposited on ITO/SnO_2/ZnO substrates, respectively. XRD spectrums of **(e)** Control, 25 µl DIM, 50 µl DIM, 100 µl DIM, and 150 µl DIM additive perovskite films deposited on ITO/SnO_2/ZnO substrates, respectively; **(f)** Enlarge spectrum corresponding to high intense peak (200) for peak shifting analysis, **(g)** Calculated d-spacing corresponding to control, 25 µl DIM, 50 µl DIM, 100 µl DIM, and 150 µl DIM assisted perovskite films, and **(h)** FWHM, crystallite size, strain, and dislocation density of perovskite crystal, extracted with (200) peak of XRD corresponding to control, 25 µl DIM, 50 µl DIM, 100 µl DIM, and 150 µl DIM assisted perovskite films, respectively.

$$\rho = \frac{n}{D^2} \quad (5)$$

where, n is a factor, for minimal dislocation density, the value of n is almost unity.

The calculated ε and ρ values corresponding to 25 µl, 50 µl, 100 µl, and 150 µl assisted DIM perovskite films are displayed in Fig. 2 (h). It was found that ε value is firstly decreased along with increased concentration of DIM, which indicates the reduction in defect density within the perovskite film. While further increase the DIM concentration (150 µl), the value of ε is enhanced, which may be due to higher concentration of DIM that impedes the crystal features. Moreover, it has been reported that larger micro strain induces defects in the film, resulting decreased the device performance. [54,55] From equation (5), dislocation density is inversely proportional to square of crystallite size, which implies that dislocation density would be reduced with increment of crystallite size. Obviously, 100 µl DIM additive based $CsPbI_2Br$ perovskite film has the highest average crystallite size and lowest dislocation density among other films (Fig. 2 (h)). Thus, from the crystal properties analysis, it is proved that an optimal concentration of DIM (100 µl) additive enhances the perovskite film quality that could improve device performance. On the other hand, with DBM additive, crystalline properties of $CsPbI_2Br$ perovskite film are deteriorated (Fig. S7(a)). The characteristic peak (2 0 0) intensity is reduced in order of 25 µl DBM, 50 µl DBM addition, and increased with 100 µl DBM concentration, which may be owing to formation of another phase as shown in FE-SEM analysis (Fig. S5(c)). A peak shift towards higher value of 2θ is observed (Fig. S7(b)) with addition of DBM (25 µl, 50 µl, and 100 µl), which implies reduction in the lattice parameter, [56] because of filling the halide vacancies by Br^- with lower ionic radii (196 pm) as compared to I^- (220 pm). Therefore, with addition of DBM, defect density is increased within the $CsPbI_2Br$ perovskite film, and it is predicted that device performance would be reduced. In case of DCM additive (25 µl, and 50 µl), crystallinity of $CsPbI_2Br$ perovskite film is increased (Fig. S8(a)) and a negligible peak (2 0 0) shift is observed towards the lower value of 2θ (Fig. S8(b)). It was reported that Cl^- ions passivates the surface defects and increase the perovskite film properties. [47] Thus, it seems that device performance would be increased with certain amount of DCM additive.

To identify the influence of DIM, DBM and DCM liquid additives on optoelectronic properties of $CsPbI_2Br$ perovskite film, ultraviolet visible (UV–vis) and photoluminescence (PL) spectrums were carried out. The obtained absorption patterns for DIM, DBM and DCM additives based $CsPbI_2Br$ perovskite films are shown in Fig. 3 (a), Fig. S9 (a) and Fig. S10 (a) respectively. From Fig. 3(a), the absorption peak for control perovskite film was found near 627 nm, which is consistent with other report. [28] For DIM (25 µl, 50 µl, and 100 µl) additive-based perovskite films, absorption onset was shifted to longer wavelength (red shift), due to addition of DIM that contains I^- ions, fills the halide ion vacancies or replaces the Br^- ion position in the perovskite lattice, resulting

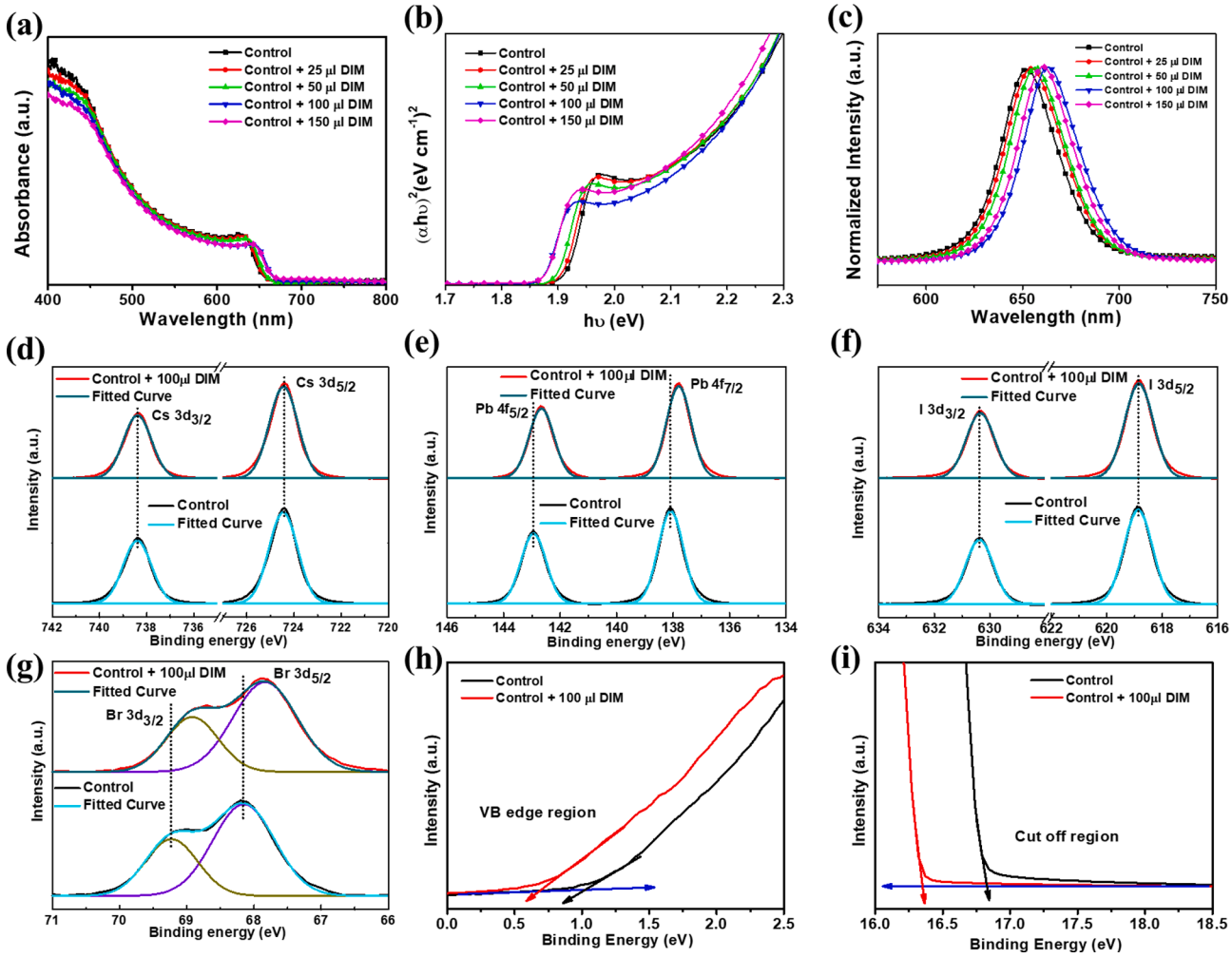

Fig. 3. **(a)** UV–vis spectrums, **(b)** Tauc plots for Control, 25 µl DIM, 50 µl DIM, 100 µl DIM, and 150 µl DIM additive perovskite films and **(c)** PL spectrums for Control, 25 µl DIM, 50 µl DIM, 100 µl DIM, and 150 µl DIM additive perovskite films; High resolution XPS spectrums of **(d)** Cs 3d, **(e)** Pb 4f, **(f)** I 3d **(g)** Br 3d core levels for control and 100 µl DIM perovskite films; and UPS patterns **(h)** VB edge and, **(i)** Cut-off region corresponding to control and 100 µl DIM perovskite films, respectively.

concentration of I^- ions increasing within the perovskite film, reducing the optical band gap of the perovskite film.

Moreover, with increasing the concentration of DIM, a gradual decrement in absorption peak intensity is observed, owing to reduction in thickness of perovskite film as shown in cross section FE-SEM image (Fig. 2(d)). The DIM is a liquid additive into the perovskite precursor solution. This approach decreases the concentration of pristine perovskite precursor solution, which affects reduction in the formed final film thickness.

The optical band gaps (E_g) correspond to control, DIM additives (25 µl, 50 µl, 100 µl, and 150 µl) based perovskite were calculated using Tauc plots (Fig. 3 (b)) and obtained E_g values were found to 1.915, 1.907, 1.899, 1.874, and 1.877 eV, respectively. The optical band gap (~1.915 eV) of control perovskite film is close to reported value (1.910 eV), [57] and E_g values exhibit a decreasing trend with increasing the concentration of DIM. In case of DBM (Fig. S9(a)), it is clearly observed that absorption peak intensity reduced, and absorption onset shift to lower wavelength (blue shift), that means, the value of E_g increased in order of 25 µl, 50 µl, and 100 µl DBM concentration assisted perovskite films. The increment in the optical band edge with DBM additive clearly suggests that Br^- ions concentration increased within the perovskite film. Thus, DIM and DBM liquid additives regulate the optoelectronic properties of α-$CsPbI_2Br$ by varying the halide ions composition within the perovskite film. On the other hand, addition of DCM with different concentrations (25 µl, 50 µl, 100 µl, and 150 µl) allows for the minor shift in the absorption onset of control perovskite film (Fig. S10(a)), because incorporation of Cl^- ions improves the film quality without affecting the optoelectronic properties, [58] which is consistent with our results. Moreover, absorption intensity is gradually reduced with increasing the concentration of DCM, because DCM is liquid additive that would affect the film thickness. In addition, PL spectrums correspond to DIM, DBM and DCM additives based $CsPbI_2Br$ perovskite films are shown in Fig. 3(c), Fig. S9(b) and Fig. S10(b), respectively. From Fig. 3(c), it was clearly observed that as increasing the concentration of DIM (25 µl, 50 µl, and 100 µl), an emission peak was shifted to longer wavelength (red shift) owing to increment in iodide ions, which is consistent with UV–vis analysis. While further increase concentration to 150 µl, a reverse trend was observed; and emission peak was shifted to lower wavelength, which also indicated that at higher concentration of DIM, crystal features were distorted as compared to 100 µl DIM. On the other hand, emission peak was shifted to shorter wavelength (blue shift) with increasing the concentration of DBM (25 µl, 50 µl, and 100 µl) (Fig. S9(b)), due to increment in Br^- ions. Notably, at 100 µl DBM, an emission peak with low intensity was found near 734 nm, which may be owing to formation of secondary phase as revealed in FE-SEM analysis (Fig. S5(c)). In case of DCM (Fig. S10(b)), a negligible peak shift to lower wavelength is observed, which is consistent with UV–vis analysis.

Furthermore, to understand the interaction of DIM (100 µl) with $CsPbI_2Br$ perovskite, XPS measurement was performed and obtained broad scan patterns were displayed in Fig. S11. The X-ray source energy (Al Kα (photon energy = 1486.6 eV) in vacuum ($\sim 5 \times 10^{-8}$)) was used to obtain XPS patterns. The obtained patterns were calibrated with C1s (284.8 eV) and fitted using gaussian function (Coefficient of determination (COD(R2)) = 0.9980 ~ 0.9946, Total Iterations = 5) with background subtraction. The high-resolution spectra corresponding to Cs, Pb, I and Br core levels were depicted in Fig. 3(d-g). The control $CsPbI_2Br$ perovskite film showed Cs, Pb, I and Br core levels at characteristics binding energies which is consistent with other reports. [34,35] The position of core level (Cs, Pb, I and Br) peaks corresponding to $CsPbI_2Br$, and DIM assisted $CsPbI_2Br$ perovskite films were depicted in Table S1. It is clearly observed that, with addition of DIM, a shift in chemical bonding states (Pb and Br) was observed, which manifests that DIM interacted with $CsPbI_2Br$. Notably, high resolution Pb spectra displayed two peaks (Pb $4f_{7/2}$: 143.0 eV, Pb $4f_{5/2}$: 138.1 eV) were shifted to lower binding energies (Pb $4f_{7/2}$: 142.7 eV, Pb $4f_{5/2}$: 137.8 eV) as shown in Fig. 3(e), which revealed that DIM is passivating the uncoordinated Pb^{2+} dangling bonds. The quantitative analysis for Pb 4f and I 3d are shown in Table S2 and it is clearly revealed atomic percentage of I 3d increased with DIM additive that plays a crucial role to mitigates the halide vacancies. Moreover, by normalizing the pattern with respect to Pb 4f peak, we calculated the I/Pb ratio for control and DIM treated perovskite films as shown in Fig. S12. For control perovskite film, average I/Pb ratio was ~ 1.8, which is lower than the theoretical value of 2, suggesting the deficiency or vacancies of iodide ions on the perovskite surface. However, after the DIM additive, average I/Pb ratio was increased to 1.94, which is much closer to the theoretical value, indicating that iodide ions vacancies are effectively filled with addition of DIM. Thus, improvement in I/Pb ratio suggested that halide ions vacancies defects were effectively suppressed with DIM additive. The deconvoluted peaks associated with Br (Br $3d_{5/2}$: 68.2 eV, Br $3d_{3/2}$: 69.0 eV) also shifted to lower binding energies (Br $3d_{5/2}$: 67.9 eV, Br $3d_{3/2}$: 68.7 eV) with addition of DIM as depicted in Fig. 3 (g), which may be owing to filling of halide vacancies with iodide ions. Moreover, Br 3d spectra shift to lower binding energies implies that electron density around the Br surface species is altered, [59] indicating strong interaction between DIM and perovskite.

Moreover, to elucidate the effect of DIM additive on electronic structure of $CsPbI_2Br$ perovskite, valance band and conduction band positions were calculated using Ultraviolet photoelectron spectroscopy (UPS) measurement (emission energy of He irradiation = 21.22 eV) as shown in Fig. 3 (h, i). From Fig. 3(h), Fermi edge ($E_{F,edge}$) values were extracted as 0.69 eV (control) and 1.02 eV (DIM additive). Using $E_{VB} = E_F - E_{F,edge}$, [60,61] where E_F is Fermi energy level, the valance band maximum (VBM) values are determined as − 5.55 eV and − 5.39 eV for control and DIM additive perovskite films. From Fig. 3(i), $E_{cut\text{-}off}$ (Cut off binding energy) was obtained as 16.36 eV and 16.85 eV correspond to control and DIM additive perovskite films, respectively. The E_F values of control and DIM additive perovskite films were found to be − 4.86 eV and − 4.37 eV, respectively, resulting from $E_F = E_{cut\text{-}off} - 21.22$ eV. [62] According to the formula $E_{CB} = E_{VB} + E_g$, [63] conduction band position can be determined as − 3.63 eV and − 3.51 eV for control and DIM additive perovskite films. Obviously, valence band maximum (VBM) position of $CsPbI_2Br$ perovskite was upshifted with addition of DIM and is closer to VBM of hole transport layer (HTL), indicating that difference between perovskite layer and HTL VBM positions reduced. This is beneficial to minimize energy loss of hole transport or reduce interface energy barrier, leading to higher performance. [42,64] In addition, in comparison to the control film, DIM additive perovskite film showed an upward shift in E_F relative to correspond VBM, implying that *n*-type nature is enhanced within the perovskite film. [65] Consequently, built in potential is buttressed among *n*-type perovskite and p-type HTL, which aids to separation and transport of photogenerated charge carriers within the device. [42] Thus, with DIM additive-based PSC, it is expected that device performance would be improved owing to matched band energy alignment that can suppress the interfacial charge recombination.

To investigate the effectiveness of DIM, DBM, and DCM liquid additives on photovoltaic performance, PSCs are fabricated with a configuration ITO/SnO_2/ZnO/perovskite/Poly (3-hexylthiophene-2,5-diyl)/Au as demonstrated in schematic diagram (Fig. 4 (a)). The energy band alignment corresponding to device architecture was shown in Fig. 4(b). The measured current density - voltage (J-V) curves for different concentration of DIM, DBM, and DCM were shown in Fig. 4(c), Fig. S13, and Fig. S14, respectively and corresponding photovoltaic (PV) parameters were listed in Table 1, Table S3 and Table S4, respectively. It is worth to note that PV parameters significantly influenced with addition of DIM, DBM, and DCM. The control PSC exhibits a PCE of 13.95 % with J_{SC} of 14.80 mA/cm^2, open circuit voltage (V_{OC}) of 1218 mV, and fill factor (FF) of 77.38 %. Notably, with an optimum concentration of DIM (100 µl) based PSC, PV parameters significantly enhanced as PCE of 16.42 %, short circuit current density (J_{SC}) of 16.11 mA/cm^2, V_{OC} of 1236 mV, and FF of 82.47 % and considered to be a champion device. It

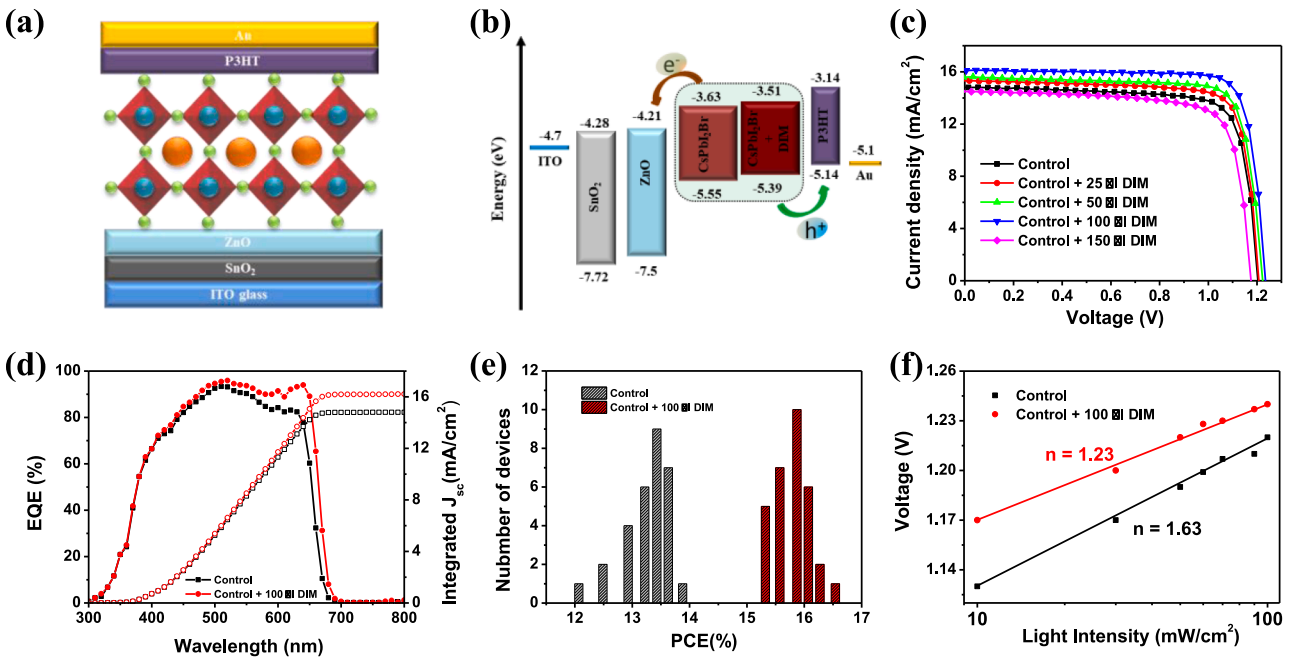

Fig. 4. **(a)** Schematic of device structure, **(b)** Schematic of energy band alignment corresponding to device architecture **(c)** J-V curves for control, 25 µl DIM, 50 µl DIM, 100 µl DIM, and 150 µl DIM additives-based PSCs, **(d)** EQE and Integrated J_{SC}, **(e)** Histogram of PCEs distribution corresponding to control, and 100 µl DIM assisted PSCs and **(h)** V_{OC} versus light intensity.

Table 1
Photovoltaic parameters of control, 25 µl DIM, 50 µl DIM, 100 µl DIM, and 150 µl DIM additives-based PSCs.

Devices		J_{SC} (mA/cm^2)	V_{OC} (mV)	FF (%)	PCE (%)
Control	Champion	14.80	1218	77.38	13.95
	Average	14.45 ± 0.34	1194 ± 22	76 ± 1.30	13.11 ± 0.79
Control + 25 µl DIM	Champion	15.33	1220	79.13	14.80
	Average	15.00 ± 0.30	1198 ± 20	77.90 ± 1.20	14.01 ± 0.73
Control + 50 µl DIM	Champion	15.62	1226	80.15	15.35
	Average	15.34 ± 0.28	1200 ± 22	78.80 ± 1.22	14.51 ± 0.74
Control + 100 µl DIM	Champion	16.11	1236	82.47	16.42
	Average	15.90 ± 0.20	1216 ± 18	81.30 ± 1.15	15.75 ± 0.67
Control + 150 µl DIM	Champion	14.48	1190	76.00	13.09
	Average	14.00 ± 0.40	1165 ± 24	74.60 ± 1.30	12.15 ± 0.90

is noteworthy that our air processed champion device (100 µl DIM) PCE of 16.42 % is highest till date based on purely additive engineering as compared to reported photovoltaic performances (Table S5) under ambient conditions. In contrast to control device, the enhancement in J_{SC} suggests that photo-carrier loss at perovskite/HTL interface is greatly mitigated owing to well matched band energy (Fig. 4(b)). A suitable band energy level facilitates efficient transportation of photo-carriers, resulting enhancement in the charge collection efficiency. The impressive improvement in FF indicates that nonradiative recombination centers associated with defects within the perovskite film were strongly suppressed due to formation of high-quality perovskite film, which is consistent with FE-SEM and XRD analysis. On the other hand, DBM additive deteriorated the film quality, resulting reduced the device performance (Fig. S13). In case of DCM, with 25 µl concentration of DCM, device performance is enhanced (Fig. S14), because Cl^- ion passivates the defects within the perovskite film that leading to higher performance.

Moreover, the external quantum efficiency (EQE) measurement is performed to calculate integrated J_{SC} for control and champion PSC. As obtained EQE spectra are shown in Fig. 4(d), the integrated J_{SC} values were found to be 14.81 mA/cm^2 and 16.11 mA/cm^2 corresponding to control and 100 µl DIM additive-based PSC, respectively. Those are in good agreement with the J_{SC} values as obtained from J-V measurements with negligible deviation (less than ~ 5 %), confirming the accuracy of J-V curves. Additionally, in case of 100 µl DIM, EQE spectra exhibited the red shift, which is consistent with UV–vis and PL results. To examine reproducibility, 30 individual devices were constructed and obtained PCE is displayed in Fig. 4(e). It was found that 100 µl DIM additive-based devices exhibited narrow PCE distribution, which elucidates good reproducibility as compared to control PSCs.

The device reliability was further estimated by conducting steady-state power output measurement at maximum power point (MPP) under 1-sun illumination in ambient conditions for control and 100 µl DIM based PSCs. As shown in Fig. S15, the stabilized power output (SPO) is maximum with 100 µl DIM assisted PSC as compared to control device and constant over 300 s, which manifests the better operational stability with DIM additive. To identify the change of environmental humidity effect on device performance, we have fabricated target device (control + 100 µl DIM) under different environmental humid conditions and analyzed its performance. The obtained current density (J-V) curves were showing in Fig. S16, and corresponding photovoltaic parameters listed in Table S6. The champion device PCE is almost similar up to ~ 40 % relative humidity (RH). When RH increases more than 40 %, device PCE began to be slightly degraded. With further humidity increases more than 50 %, the performance of device was noticeably affected by probable moisture penetration.

To recognize charge recombination phenomena, V_{OC} as a function of illumination intensity is examined by plotting V_{OC} versus light intensity logarithmically, and obtained curves were shown in Fig. 4(f). The slope of fitted curve is used to calculate ideality factor (η) by following equation: [66,67]

$$V_{OC} = \eta \frac{k_B T}{q} ln(I) + constant \quad (6)$$

From above equation, η value can be determined as:

$$\eta = slope \times \frac{k_B T}{q} \quad (7)$$

where, k_B is Boltzmann constant, T is temperature (K), q is elementary charge, and I is light intensity. The η is ideality factor that identify the dominance of recombination mechanisms in the perovskite solar cells, where value of ideality factor as η = 1 signifies the bimolecular recombination, and η = 2 indicates the trap-assisted recombination. [68–70]

The η values were calculated to be 1.63 and 1.23 correspond to control and 100 µl DIM-PSC, respectively. Comparatively, DIM based PSC exhibited smaller value of η, which suggests that trap assisted recombination could be effectively suppressed, [1,67] consistent with FE-SEM and XRD results. Moreover, the significant improvement in device FF (77 % to 82.47 %) also suggests the efficient charge extraction by reducing the traps, with addition of DIM.

In addition, to further investigate the effect of DIM additive on trap-state density, space charge limited current (SCLC) measurement was conducted to quantitatively assess the trap density within the fabricated perovskite films. The dark J-V curves for control and 100 µl DIM assisted PSCs were measured (Fig. 5 (a, b) by constructing electron-only device with structure (ITO/SnO_2/ZnO/perovskite/Phenyl-C61-butyric acid methyl ester/Au). As depicted in Fig. 5 (a, b), the trap-filled limited voltage (V_{TFL}) was measured at the kink point, which shows the transition from ohmic region to trap-filled limited region. The trap density can be estimated using the following equation: [61]

$$V_{TFL} = \frac{e n_t L^2}{2 \varepsilon_r \varepsilon_0} \quad (8)$$

where, e is electric charge, n_t is defect density, L is the thickness of the film, ε_r is relative dielectric constant (ε_r = 8.5 for $CsPbI_2Br$), [27] and ε_0 is vacuum permittivity. The V_{TFL} values for control (Fig. 5 (a)) and 100 µl DIM-PSC (Fig. 5 (b)) are found to be 0.96 V and 0.43 V, respectively. Accordingly, n_t values deduced to be 5.3 × 10^{15} cm^{-3} and 2.9 × 10^{15} cm^{-3} for control and 100 µl DIM-PSCs, respectively. As a result, the trap density remarkably suppressed in case of DIM assisted PSC, implies that addition of DIM plays the key role to mitigate the defects by passivating uncoordinated Pb^{2+} dangling bonds. The numerous research studies have been suggested that rough surface with pinholes or grain boundaries induced the shallow trap states, which act as recombination centers in the PSCs. [35,71] Thus, the low trap density associated with DIM assisted perovskite film indicates that crystalline quality of perovskite was improved, and hence loss of photo-carrier at recombination centers effectively diminished.

Furthermore, the dark J-V curves were measured for control and DIM assisted PSC as displayed in Fig. 5(c). Clearly, DIM assisted PSC shows lower value of leakage current as compared to control device, and it also entails that DIM additive lessens the defects within the perovskite film. It was found that leakage current originated from existed pinholes and grain boundaries in the perovskite film. [35] Thus, a smaller value of dark current signifies that a low number of defects are presented. [35,72]

To gain deep insight into charge carrier transfer and recombination kinetics within the PSCs, transient photovoltage (TPV) and transient photocurrent (TPC) decays were recorded. From Fig. 5 (d) (TPV), the charge carrier recombination lifetimes were determined to be 21.1 µs and 58.2 µs, corresponding to control and DIM assisted PSCs, respectively. Conspicuously, carrier lifetime is enhanced with addition of DIM, which suggests that non-radiative recombination strongly suppressed. The slower decay in TPV result indicates recombination time (τ_{rec}) was increased by reducing trap states, leading to higher performance. [9] As shown in Fig. 5(e) (TPC), the charge transport lifetime (τ_{ct}) of 100 µl DIM assisted PSC (1.49 µs) was shorter than control (2.49 µs), which signifies quicker charge carrier extraction and transportation in case of the cell with DIM additive owing to the matched band energy alignment and defect passivation. The faster TPC decay time is attributed to the high-quality perovskite film which facilitates efficient charge extraction and transport process. Simultaneously, to reveal the favourable impact of DIM on charge carrier recombination dynamics, electrochemical impedance spectroscopy (EIS) test was performed under dark conditions in the frequency range of 100 Hz to 2 MHz with 1.0 V applied voltage. The obtained Nyquist plots for control and DIM assisted PSCs are shown

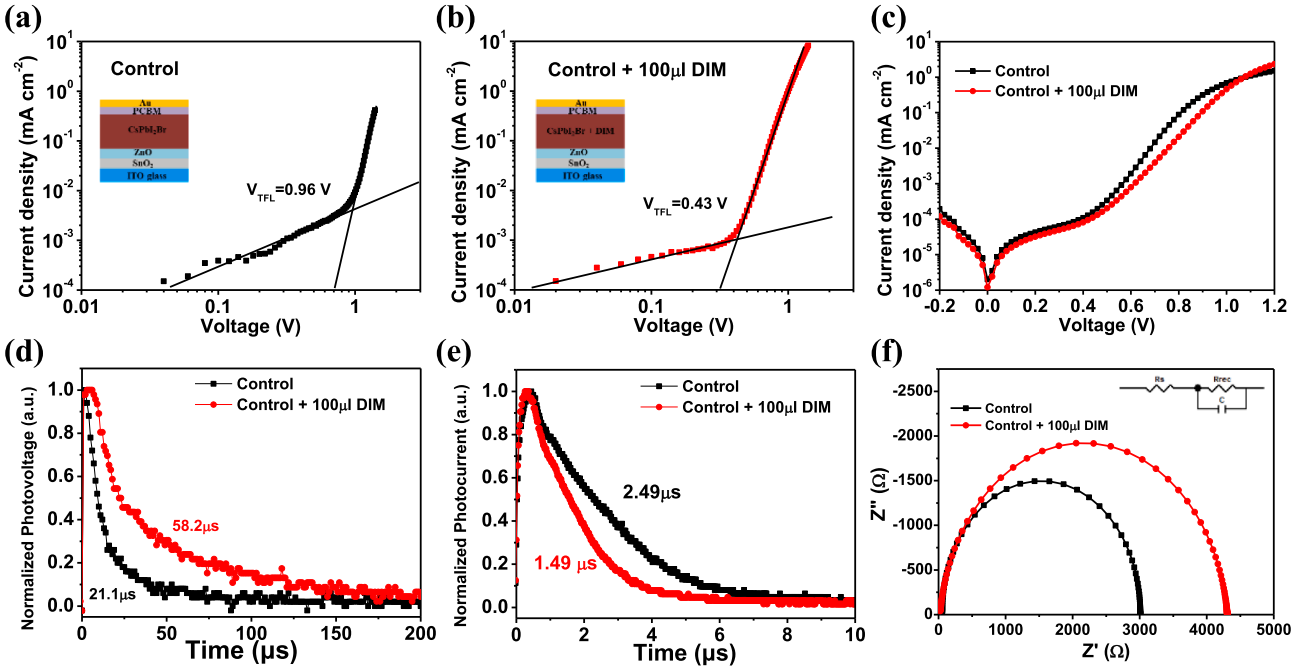

Fig. 5. SCLC measurements **(a)** Control, and **(b)** 100 µl DIM assisted PSCs; **(c)** dark J-V, **(d)** transient photovoltage (TPV), **(e)** transient photocurrent (TPC) and **(f)** electrochemical impedance spectroscopy (EIS) spectrums for control and 100 µl DIM assisted PSCs.

in Fig. 5(f). The curves were fitted with Z-view software according to equivalent circuit model as shown in inset of Fig. 5(f) and obtained Nyquist parameters are shown in Table S7. The DIM assisted PSC exhibited lower value (27.92 Ω) of series resistance as compared to control PSC (34.0 Ω), which suggested that defects were passivated through DIM additive. Moreover, EIS semicircle middle frequency zone was dictated by recombination resistance (R_{rec}) corresponding to charge transport layer (CTL)/perovskite interface. [73] The value of R_{rec} can be extracted in the low frequency region related to diameter of EIS semicircle and intercept on the X-axis (Z'(Ω)). [74] The R_{rec} values for control and 100 µl DIM assisted PSCs are determined to be 2800 Ω and 4303 Ω, respectively. Notably, DIM assisted PSC exhibited higher value of R_{rec} as compared to control device, which confirmed that charge carrier recombination remarkably suppressed, which is consistent with SCLC and TPV results. Thus, it can be clearly revealed from above characterization results that DIM additive notably enhanced the device performance by suppressing notorious photo carrier recombination.

Apart from device performance, ambient stability is another serious concern as associated with inorganic $CsPbI_2Br$ PSC. The presence of pin holes, voids, grain boundaries, and rough surface is vigorously unstable and most vulnerable to moisture invasion and permeation that converts photo-active phase (α-$CsPbI_2Br$) into non-perovskite phase (δ-$CsPbI_2Br$), resulting degradation in the device PCE. [75] Thus, it is urgent to fabricate high quality perovskite film with preferred crystal features. In this regard, DIM additive plays a vital role to fabricate high quality perovskite film with uniform surface. To examine the long-term air stability, control and 100 µl DIM assisted PSCs without any encapsulation are kept under ambient conditions (RH range of 20 to 32 % and temperature range of 20 to 24 °C) and obtained result is depicted in Fig. 6 (a). It has been found that control PSC reduced steadily, reaching to ~ 52 % of original PCE after aging 600 hrs under ambient conditions, while 100 µl DIM assisted PSC maintained ~ 80 % of initial PCE value without encapsulation. In contrast, 100 µl DIM assisted PSC exhibited better ambient stability than control PSC. The improved long-term air stability of 100 µl DIM assisted PSC could be attributed to the considerably enhanced the crystal quality of $CsPbI_2Br$ perovskite film with DIM additive.

We have also monitored the long-term thermal and light stability for control and DIM assisted perovskite solar cells (PSCs) under ambient conditions (RH ~ 22 to 36 %, temperature range: 20 to 24 ℃) without any encapsulation. As shown in Fig. 6(b), DIM assisted PSC retained ~ 85 % of initial power conversion efficiency (PCE), whereas control device maintained ~ 66 % of original PCE after aging at 85℃ for 360 h. This confirms high thermal stability of the suggested device. Additionally, the photostability of control and DIM assisted PSCs was examined under continuous white light illumination (100 mW/cm^2) for 150 h as presented in Fig. 6(c). The DIM based device showed higher light stability by maintaining the ~ 65 % of its original PCE, whereas control PSC displayed ~ 34 % retention of initial PCE. Thus, DIM assisted device exhibited higher thermal and light stability as compared to control PSC.

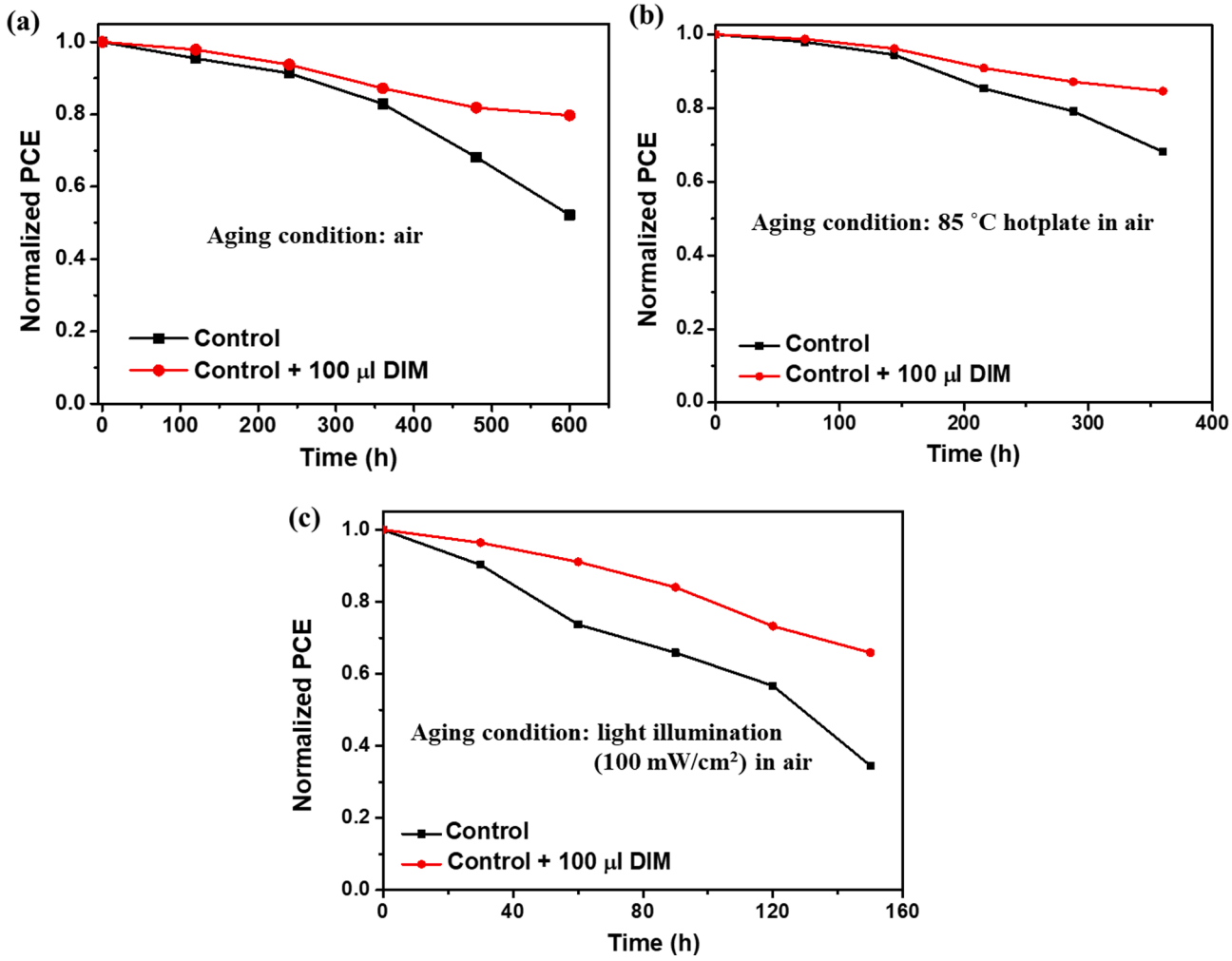

Fig. 6. **(a)** Long-term air stability of control and 100 µl DIM assisted PSCs under ambient conditions (RH range of ~ 20 to 32 % and temperature range of 20 to 24 °C), without any encapsulation, **(b)** Thermal and **(c)** Light stability of control and 100 µl DIM assisted PSCs under ambient conditions (RH range of ~ 22 to 36 % and temperature range of 20 to 24 °C), without any encapsulation.

The DIM additive aids to control the crystallization kinetics, reduces the halide ion vacancies, passivates uncoordinated Pb^{2+} dangling bond and diminishes trap density states, producing high quality perovskite film with uniform and dense surface morphology that stabilizes the device performance under thermal stress as well as in lighting conditions.

Thus, our findings demonstrated the important role of DIM additive to obtain a compact, uniform and highly crystalline $CsPbI_2Br$ perovskite film with lower defect density, which is beneficial for fabrication of efficient and stable PSCs. We believe that our strategy with additive engineering would pave promising way and encourage to research community for further development of efficient and stable all-inorganic PSCs under ambient conditions.

3. Conclusion

In summary, we successfully presented an effective approach for development of efficient inorganic $CsPbI_2Br$ PSCs under ambient conditions by employing various small carbon chain liquid additives (DIM, DBM and DCM). These additives modulate crystallization process and tune optoelectronic properties of $CsPbI_2Br$ perovskite. It has been found that DIM and DCM provide favorable impact on the $CsPbI_2Br$ film properties, leading to higher device performance. In case of DBM, $CsPbI_2Br$ perovskite film morphology was affected, resulting in decrease of the device performance. The maximum PCE of 13.95 %, 16.42 %, 12.51 %, and 14.45 % were obtained corresponding to control, 100 µl DIM, 25 µl DBM and 25 µl DCM assisted PSCs, respectively. Notably, it has been found that 100 µl DIM regulate crystallization process, facilitate preferential oriented grain growth, reduce dislocation density, match band energy alignment, reduce interface recombination, passivate uncoordinated Pb^{2+} dangling bond, halide ion vacancies and halide interstitial defects, and suppress octahedral tilting. In consequence, with the DIM additive, trap states significantly decreased as compared to control perovskite film. As a result, 100 µl DIM assisted $CsPbI_2Br$ PSC exhibited the best performance of 16.42 % which is highest till date with purely additive engineering approach under ambient air processing. Additionally, it showed better long-term stability as compared to control PSC under ambient conditions. Thus, present work shows a novel strategy for formation of high-quality perovskite film under ambient conditions (RH range of 20 to 32 % and temperature range of 20 to 24 °C) to further boost overall performance of inorganic $CsPbI_2Br$ PSCs.

CRediT authorship contribution statement

Jitendra Bahadur: Conceptualization, Methodology, Investigation, Validation, Data curation, Visualization, Formal analysis, Writing – original draft. **Jun Ryu:** Methodology, Investigation, Validation, Data curation, Visualization, Formal analysis. **Dong-Gun Lee:** Data curation. **Jongin Hong:** Data curation. **Shuzi Hayase:** Project administration. **Jung Sang Cho:** Writing – review & editing, Conceptualization, Supervision, Project administration, Funding acquisition. **Sang Mun Jeong:** Writing – review & editing, Conceptualization, Supervision, Project administration, Funding acquisition. **Dong-Won Kang:** Writing – review & editing, Conceptualization, Supervision, Project administration, Funding acquisition.

Declaration of Competing Interest

The authors declare that they have no known competing financial interests or personal relationships that could have appeared to influence the work reported in this paper.

Data availability

Data will be made available on request.

Acknowledgements

This work was supported by the National Research Foundation of Korea (NRF) grant funded by the Korea government (MSIT) (NRF - 2021R1A2C4002045, 2021R1A4A2001687, 2021K2A9A2A08000082, and 2019K1A3A1A39103051).

Appendix A. Supplementary data

Supplementary data to this article can be found online at https://doi.org/10.1016/j.apsusc.2022.156229.

References

[1] W. Tang, Y. Chen, J. Yang, R. Yuan, Y. Lv, Q. Ma, Y. Wu, P. Zhang, W.-H. Zhang, Acetone-assisted precursor engineering enables low-temperature fabrication of $CsPbI_2Br$ perovskite for efficient solar cells, J. Power Sources 482 (2021), 228965.
[2] H. Wang, H. Bian, Z. Jin, H. Zhang, L. Liang, J. Wen, Q. Wang, L. Ding, S.F. Liu, Cesium lead mixed-halide perovskites for low-energy loss solar cells with efficiency beyond 17%, Chem. Mater. 31 (2019) 6231–6238.
[3] Y.-H. Kye, C.-J. Yu, C.-H. Kim, Y.-S. Kim, U.-G. Jong, Influence of Metal-Ion Replacement on the Phase Stabilization of Cubic All-Inorganic Cesium Lead Halide Perovskites: an Ab Initio Thermodynamic Formalism for Solution-Processed Cation Doping, J. Phys. Chem. C 125 (2021) 13195–13211.
[4] A. Kojima, K. Teshima, Y. Shirai, T. Miyasaka, Organometal halide perovskites as visible-light sensitizers for photovoltaic cells, J. Am. Chem. Soc. 131 (2009) 6050–6051.
[5] National Renewable Energy Laboratory, Best Research-Cell Efficiencies Chart.
[6] M. Green, E. Dunlop, J. Hohl-Ebinger, M. Yoshita, N. Kopidakis, X. Hao, Solar cell efficiency tables (version 57), Prog. Photovolt.: Res. Appl. 29 (2021) 3–15.
[7] W. Chen, H. Chen, G. Xu, R. Xue, S. Wang, Y. Li, Y. Li, Precise control of crystal growth for highly efficient $CsPbI_2Br$ perovskite solar cells, Joule 3 (2019) 191–204.
[8] J. Tian, Q. Xue, X. Tang, Y. Chen, N. Li, Z. Hu, T. Shi, X. Wang, F. Huang, C. J. Brabec, H.-L. Yip, Dual interfacial design for efficient $CsPbI_2Br$ perovskite solar cells with improved photostability, Adv. Mater. 31 (2019) 1901152.
[9] S. Fu, J. Wang, X. Liu, H. Yuan, Z. Xu, Y. Long, J. Zhang, L. Huang, Z. Hu, Y. Zhu, Multifunctional liquid additive strategy for highly efficient and stable $CsPbI_2Br$ all-inorganic perovskite solar cells, J. Chem. Eng. 422 (2021), 130572.
[10] Q. Zeng, X. Zhang, C. Liu, T. Feng, Z. Chen, W. Zhang, W. Zheng, H. Zhang, B. Yang, Inorganic $CsPbI_2Br$ perovskite solar cells: the progress and perspective, Solar RRL 3 (2019) 1800239.
[11] Y. Zhao, J. Duan, H. Yuan, Y. Wang, X. Yang, B. He, Q. Tang, Using SnO_2 QDs and CsMBr 3 (M= Sn, Bi, Cu) QDs as charge-transporting materials for 10.6%-efficiency all-inorganic $CsPbB_r3$ perovskite solar cells with an ultrahigh open-circuit voltage of 1.610 V, Solar RRL 3 (2019) 1800284.
[12] S.M. Yoon, H. Min, J.B. Kim, G. Kim, K.S. Lee, S.I. Seok, Surface engineering of ambient-air-processed cesium lead triiodide layers for efficient solar cells, Joule 5 (2021) 183–196.
[13] X. Wang, Y. Wang, Y. Chen, X. Liu, Y. Zhao, Efficient and stable $CsPbI_3$ inorganic perovskite photovoltaics enabled by crystal secondary growth, Adv. Mater. 33 (2021) 2103688.
[14] J. Wang, L. Chen, Z. Qian, G. Ren, J. Wu, H. Zhang, Optimal intermediate adducts regulate low-temperature $CsPbI_2Br$ crystallization for efficient inverted all-inorganic perovskite solar cells, J. Mater. Chem. A 8 (2020) 25336–25344.
[15] Z. Wang, A.K. Baranwal, P. Zhang, G. Kapil, T. Ma, S. Hayase, Delocalized molecule surface electronic modification for enhanced performance and high environmental stability of CsPbI2Br perovskite solar cells, Nano Energy 66 (2019), 104180.
[16] Z. Guo, A.K. Jena, I. Takei, G.M. Kim, M.A. Kamarudin, Y. Sanehira, A. Ishii, Y. Numata, S. Hayase, T. Miyasaka, V_{OC} Over 1.4 V for Amorphous Tin-Oxide-Based Dopant-Free $CsPbI_2Br$ Perovskite Solar Cells, J. Am. Chem. Soc. 142 (2020) 9725–9734.
[17] Z. Guo, A.K. Jena, I. Takei, M. Ikegami, A. Ishii, Y. Numata, N. Shibayama, T. Miyasaka, Dopant-Free Polymer HTM-Based $CsPbI_2Br$ Solar Cells with Efficiency Over 17% in Sunlight and 34% in Indoor Light, Adv. Funct. Mater. 31 (2021) 2103614.
[18] W. Chen, X. Li, Y. Li, Y. Li, A review: crystal growth for high-performance all-inorganic perovskite solar cells, Energy Environ. Sci. 13 (2020) 1971–1996.
[19] Y. Wang, T. Zhang, M. Kan, Y. Li, T. Wang, Y. Zhao, Efficient α-$CsPbI_3$ photovoltaics with surface terminated organic cations, Joule 2 (2018) 2065–2075.
[20] A. Rajagopal, K. Yao, A.K.Y. Jen, Toward perovskite solar cell commercialization: a perspective and research roadmap based on interfacial engineering, Adv. Mater. 30 (2018) 1800455.
[21] T. Tong, X. Li, S. Guo, J. Han, B. Wei, Sequential solvent processing with hole transport materials for improving efficiency of traditionally-structured perovskite solar cells, Nano Energy 41 (2017) 591–599.
[22] X. Zheng, Y. Deng, B. Chen, H. Wei, X. Xiao, Y. Fang, Y. Lin, Z. Yu, Y. Liu, Q. Wang, J. Huang, Dual functions of crystallization control and defect passivation enabled by sulfonic zwitterions for stable and efficient perovskite solar cells, Adv. Mater. 30 (2018) 1803428.
[23] K.-L. Wang, R. Wang, Z.-K. Wang, M. Li, Y. Zhang, H. Ma, L.-S. Liao, Y. Yang, Tailored phase transformation of $CsPbI_2Br$ films by copper (II) bromide for high-performance all-inorganic perovskite solar cells, Nano Lett. 19 (2019) 5176–5184.

[24] D. Bai, J. Zhang, Z. Jin, H. Bian, K. Wang, H. Wang, L. Liang, Q. Wang, S.F. Liu, Interstitial Mn^{2+}-driven high-aspect-ratio grain growth for low-trap-density microcrystalline films for record efficiency $CsPbI_2Br$ solar cells, ACS Energy Lett. 3 (2018) 970–978.

[25] C.F.J. Lau, M. Zhang, X. Deng, J. Zheng, J. Bing, Q. Ma, J. Kim, L. Hu, M.A. Green, S. Huang, Strontium-doped low-temperature-processed $CsPbI_2Br$ perovskite solar cells, ACS Energy Lett. 2 (2017) 2319–2325.

[26] S. Yang, H. Zhao, Y. Han, C. Duan, Z. Liu, S. Liu, Europium and acetate Co-doping strategy for developing stable and efficient $CsPbI_2Br$ perovskite solar cells, Small 15 (2019) 1904387.

[27] H. Sun, J. Zhang, X. Gan, L. Yu, H. Yuan, M. Shang, C. Lu, D. Hou, Z. Hu, Y. Zhu, L. Han, Pb-reduced $CsPb_{0.9}Zn_{0.1}I_2Br$ thin films for efficient perovskite solar cells, Adv. Energy Mater. 9 (2019) 1900896.

[28] F. He, W. Xu, M. Zhang, X. Zhang, B. Ding, G. Wei, F. Kang, Highly crystalline $CsPbI_2Br$ films for efficient perovskite solar cells via compositional engineering, RSC Adv. 9 (2019) 30534–30540.

[29] J. Li, G. Zhang, Z. Zhang, J. Li, Z. Uddin, Y. Zheng, Y. Shao, Y. Yuan, B. Yang, Defect Passivation via Additive Engineering to Improve Photodetection Performance in $CsPbI_2Br$ Perovskite Photodetectors, ACS Appl. Mater. Interfaces 13 (2021) 56358–56365.

[30] S. Oz, A.K. Jena, A. Kulkarni, K. Mouri, T. Yokoyama, I. Takei, F. Ünlü, S. Mathur, T. Miyasaka, Lead (II) propionate additive and a dopant-free polymer hole transport material for $CsPbI_2Br$ perovskite solar cells, ACS Energy Lett. 5 (2020) 1292–1299.

[31] G. Yin, H. Zhao, H. Jiang, S. Yuan, T. Niu, K. Zhao, Z. Liu, S.F. Liu, Precursor engineering for all-inorganic $CsPbI_2Br$ perovskite solar cells with 14.78% efficiency, Adv. Funct. Mater. 28 (2018) 1803269.

[32] B. Yu, H. Zhang, J. Wu, Y. Li, H. Li, Y. Li, J. Shi, H. Wu, D. Li, Y. Luo, Q. Meng, Solvent-engineering toward $CsPb(I_xBr_{1-x})3$ films for high-performance inorganic perovskite solar cells, J. Mater. Chem. A 6 (2018) 19810–19816.

[33] C. Dong, X. Han, W. Li, Q. Qiu, J. Wang, Anti-solvent assisted multi-step deposition for efficient and stable carbon-based $CsPbI_2Br$ all-inorganic perovskite solar cell, Nano Energy 59 (2019) 553–559.

[34] L. Yu, T. Guo, H. Yuan, Z. Zhang, Z. Deng, R. Zhao, M. Zheng, J. Zhang, W. Xu, X. Liu, Z. Hu, Y. Zhu, Effective lewis base additive with S-donor for efficient and stable $CsPbI_2Br$ based perovskite solar cells, J. Chem. Eng. 420 (2021), 129931.

[35] H. Li, X. Hao, B. Chang, Z. Li, L. Wang, L. Pan, X. Chen, L. Yin, Stiffening the Pb-X Framework through a π-Conjugated Small-Molecule Cross-Linker for High-Performance Inorganic $CsPbI_2Br$ Perovskite Solar Cells, ACS Appl. Mater. Interfaces 13 (2021) 40489–40501.

[36] H. Peng, M. Cai, J. Zhou, Y. Yang, X. Ding, Y. Tao, G. Wu, X. Liu, J.H. Pan, S. Dai, Structurally Reinforced All-Inorganic $CsPbI_2Br$ Perovskite by Nonionic Polymer via Coordination and Hydrogen Bonds, Solar RRL 4 (2020) 2000216.

[37] L. Yan, Q. Xue, M. Liu, Z. Zhu, J. Tian, Z. Li, Z. Chen, Z. Chen, H. Yan, H.L. Yip, Interface engineering for all-inorganic $CsPbI_2Br$ perovskite solar cells with efficiency over 14%, Adv. Mater. 30 (2018) 1802509.

[38] U. Khan, T. Iqbal, M. Khan, R. Wu, SnO_2/ZnO as double electron transport layer for halide perovskite solar cells, Sol. Energy 223 (2021) 346–350.

[39] C.-C. Chueh, C.-Y. Liao, F. Zuo, S.T. Williams, P.-W. Liang, A.-K.-Y. Jen, The roles of alkyl halide additives in enhancing perovskite solar cell performance, J. Mater. Chem. A 3 (2015) 9058–9062.

[40] R.G. Pearson, Absolute electronegativity and hardness: application to inorganic chemistry, Inorganic chemistry 27 (1988) 734–740.

[41] R.G. Pearson, Hard and soft acids and bases, J. Am. Chem. Soc. 85 (1963) 3533–3539.

[42] Y. Han, H. Zhao, C. Duan, S. Yang, Z. Yang, Z. Liu, S.F. Liu, Controlled n-doping in air-stable $CsPbI_2Br$ perovskite solar cells with a record efficiency of 16.79%, Adv. Funct. Mater. 30 (2020) 1909972.

[43] B. Yang, J. Keum, O.S. Ovchinnikova, A. Belianinov, S. Chen, M.-H. Du, I. N. Ivanov, C.M. Rouleau, D.B. Geohegan, K. Xiao, Deciphering halogen competition in organometallic halide perovskite growth, J. Am. Chem. Soc. 138 (2016) 5028–5035.

[44] M.I. Dar, N. Arora, P. Gao, S. Ahmad, M. Grätzel, M.K. Nazeeruddin, Investigation regarding the role of chloride in organic–inorganic halide perovskites obtained from chloride containing precursors, Nano Lett. 14 (2014) 6991–6996.

[45] C. Gao, Z. Hu, C. Yang, H. Xu, Y. Wang, H. Zhang, J. Zhang, Y. Zhu, J. Wang, High-temperature induced iodide and bromide ions filling lattice for high efficient all-inorganic perovskite solar cells, J. Alloys Compd. 848 (2020), 156247.

[46] S.S. Mali, J.V. Patil, C.K. Hong, Hot-air-assisted fully air-processed barium incorporated $CsPbI_2Br$ perovskite thin films for highly efficient and stable all-inorganic perovskite solar cells, Nano Lett. 19 (2019) 6213–6220.

[47] L. Atourki, M. Bernabé, M. Makha, K. Bouabid, M. Regragui, A. Ihlal, M. Abd-lefdil, M.J.R.A. Mollar, Effect of doping on the phase stability and photophysical properties of $CsPbI_2Br$ perovskite thin films 11 (2021) 1440–1449.

[48] J.K. Nam, M.S. Jung, S.U. Chai, Y.J. Choi, D. Kim, J.H. Park, Unveiling the crystal formation of cesium lead mixed-halide perovskites for efficient and stable solar cells, J. Phys. Chem. Lett. 8 (2017) 2936–2940.

[49] M. Tai, Y. Zhou, X. Yin, J. Han, Q. Zhang, Y. Zhou, H. Lin, In situ formation of a 2D/3D heterostructure for efficient and stable $CsPbI_2Br$ solar cells, J. Mater. Chem. A 7 (2019) 22675–22682.

[50] F. Haque, M. Wright, M.A. Mahmud, H. Yi, D. Wang, L. Duan, C. Xu, M.B. Upama, A. Uddin, Effects of hydroiodic acid concentration on the properties of $CsPbI_3$ perovskite solar cells, ACS omega 3 (2018) 11937–11944.

[51] S. Khalid, M.A. Malik, D.J. Lewis, P. Kevin, E. Ahmed, Y. Khan, P. O'Brien, Transition metal doped pyrite (FeS_2) thin films: structural properties and evaluation of optical band gap energies, J. Mater. Chem. C 3 (2015) 12068–12076.

[52] Y. Kumar, E. Regalado-Pérez, A.M. Ayala, N. Mathews, X. Mathew, Effect of heat treatment on the electrical properties of perovskite solar cells, Sol. Energy Mater. Sol. Cells 157 (2016) 10–17.

[53] I. Robinson, R. Harder, Coherent X-ray diffraction imaging of strain at the nanoscale, Nat. Mater. 8 (2009) 291–298.

[54] G. Kapil, T. Bessho, C.H. Ng, K. Hamada, M. Pandey, M.A. Kamarudin, D. Hirotani, T. Kinoshita, T. Minemoto, Q. Shen, T. Toyoda, T.N. Murakami, H. Segawa, S. Hayase, Strain relaxation and light management in tin–lead perovskite solar cells to achieve high efficiencies, ACS Energy Lett. 4 (2019) 1991–1998.

[55] S. Lee, J. Ryu, S.S. Park, S. Yoon, D.-G. Lee, J. Moon, Y.J. Kim, D.-W. Kang, A self-assembled hierarchical structure to keep the 3D crystal dimensionality in n-butylammonium cation-capped Pb–Sn perovskites, J. Mater. Chem. A 9 (2021) 27541–27550.

[56] Q. Jiang, L. Liang, D. Zhao, Lattice contraction and surface stress of fcc nanocrystals, J. Phys. Chem. B 105 (2001) 6275–6277.

[57] J. Zhang, D. Bai, Z. Jin, H. Bian, K. Wang, J. Sun, Q. Wang, S.F. Liu, 3D–2D–0D interface profiling for record efficiency all-inorganic $CsPbBr_{i}2$ perovskite solar cells with superior stability, Adv. Energy Mater. 8 (2018) 1703246.

[58] P.W. Liang, C.Y. Liao, C.C. Chueh, F. Zuo, S.T. Williams, X.K. Xin, J. Lin, A.K. Y. Jen, Additive enhanced crystallization of solution-processed perovskite for highly efficient planar-heterojunction solar cells, Adv. Mater. 26 (2014) 3748–3754.

[59] W.S. Subhani, K. Wang, M. Du, X. Wang, S. Liu, Interface-modification-induced gradient energy band for highly efficient CsPbIBr 2 perovskite solar cells, Adv. Energy Mater. 9 (2019) 1803785.

[60] J. Chen, J.Y. Seo, N.G. Park, Simultaneous improvement of photovoltaic performance and stability by in situ formation of 2D perovskite at $(FAPbI_3)_{0.88}(CsPbBr_3)_{0.12}$/CuSCN interface, Adv. Energy Mater. 8 (2018) 1702714.

[61] J. Cao, H.L. Loi, Y. Xu, X. Guo, N. Wang, C.k. Liu, T. Wang, H. Cheng, Y. Zhu, M.G. Li, W.-Y. Wong, F. Yan, High-Performance Tin–Lead Mixed-Perovskite Solar Cells with Vertical Compositional Gradient, Adv. Mater., 34 (2022) 2107729.

[62] M. Park, J.-Y. Kim, H.J. Son, C.-H. Lee, S.S. Jang, M.J. Ko, Low-temperature solution-processed Li-doped SnO_2 as an effective electron transporting layer for high-performance flexible and wearable perovskite solar cells, Nano Energy 26 (2016) 208–215.

[63] J. Chen, X. Zhao, S.G. Kim, N.G. Park, Multifunctional chemical linker imidazoleacetic acid hydrochloride for 21% efficient and stable planar perovskite solar cells, Adv. Mater. 31 (2019) 1902902.

[64] W. Xu, F. He, M. Zhang, P. Nie, S. Zhang, C. Zhao, R. Luo, J. Li, X. Zhang, S. Zhao, Minimizing voltage loss in efficient all-inorganic $CsPbI_2Br$ perovskite solar cells through energy level alignment, ACS Energy Lett. 4 (2019) 2491–2499.

[65] X. Yang, Y. Fu, R. Su, Y. Zheng, Y. Zhang, W. Yang, M. Yu, P. Chen, Y. Wang, J. Wu, D. Luo, Y. Tu, L. Zhao, Superior carrier lifetimes exceeding 6 μs in polycrystalline halide perovskites, Adv. Mater. 32 (2020) 2002585.

[66] S.S. Mali, J.V. Patil, J.A. Steele, S.R. Rondiya, N.Y. Dzade, C.K. Hong, Implementing dopant-free hole-transporting layers and metal-incorporated $CsPbI_2Br$ for stable all-inorganic perovskite solar cells, ACS Energy Lett. 6 (2021) 778–788.

[67] J. Ma, M. Qin, Y. Li, T. Zhang, J. Xu, G. Fang, X. Lu, Guanidinium doping enabled low-temperature fabrication of high-efficiency all-inorganic $CsPbI_2Br$ perovskite solar cells, J. Mater. Chem. A 7 (2019) 27640–27647.

[68] K.-C. Hsiao, M.-H. Jao, B.-T. Li, T.-H. Lin, S.-H.-C. Liao, M.-C. Wu, W.-F. Su, Enhancing efficiency and stability of hot casting p–i–n perovskite solar cell via dipolar ion passivation, ACS Appl. Energy Mater. 2 (2019) 4821–4832.

[69] Z. Hu, Q. An, H. Xiang, L. Aigouy, B. Sun, Y. Vaynzof, Z. Chen, Enhancing the efficiency and stability of triple-cation perovskite solar cells by eliminating excess PbI2 from the perovskite/hole transport layer interface, ACS Appl. Mater. Interfaces 12 (2020) 54824–54832.

[70] T.S. Sherkar, C. Momblona, L. Gil-Escrig, J. Avila, M. Sessolo, H.J. Bolink, L.J. A. Koster, Recombination in perovskite solar cells: significance of grain boundaries, interface traps, and defect ions, ACS Energy Lett. 2 (2017) 1214–1222.

[71] Q. Hu, W. Chen, W. Yang, Y. Li, Y. Zhou, B.W. Larson, J.C. Johnson, Y.-H. Lu, W. Zhong, J. Xu, L. Klivansky, C. Wang, M.B. Salmerón, A.B. Djurišić, F. Liu, Z. He, R. Zhu, T.P. Russell, Improving efficiency and stability of perovskite solar cells enabled by a near-infrared-absorbing moisture barrier, Joule 4 (2020) 1575–1593.

[72] F. Zhang, J. Song, L. Zhang, F. Niu, Y. Hao, P. Zeng, H. Niu, J. Huang, J. Lian, Film-through large perovskite grains formation via a combination of sequential thermal and solvent treatment, J. Mater. Chem. A 4 (2016) 8554–8561.

[73] J. Xue, R. Wang, K.-L. Wang, Z.-K. Wang, I. Yavuz, Y. Wang, Y. Yang, X. Gao, T. Huang, S. Nuryyeva, J.-W. Lee, Y. Duan, L.-S. Liao, R. Kaner, Y. Yang, Crystalline liquid-like behavior: surface-induced secondary grain growth of photovoltaic perovskite thin film, J. Am. Chem. Soc. 141 (2019) 13948–13953.

[74] Y.C. Wang, J. Chang, L. Zhu, X. Li, C. Song, J. Fang, Electron-transport-layer-assisted crystallization of perovskite films for high-efficiency planar heterojunction solar cells, Adv. Funct. Mater. 28 (2018) 1706317.

[75] J.W. Lee, N.G. Park, Chemical approaches for stabilizing perovskite solar cells, Adv. Energy Mater. 10 (2020) 1903249.